Citation information: DOI: 10.1109/TCYB.2025.3626066,
IEEE TRANSACTIONS ON AEROSPACE AND ELECTRONIC SYSTEMS

Quantum-Cognitive Radar: Adaptive Detection with Entanglement under Thermal-Loss Channels

Correspondence

***Abstract*— An adaptive Quantum-Cognitive Radar (QCR), which incorporates a two-mode squeezed-vacuum (TMSV) transmitter, a joint idler-signal receiver, and a Quantum Neural Network (QNN) controller to optimize parameters in real time, is introduced through this exchange of correspondence. An expression for a Gaussian correlation detector has been found for thermal-loss channels and compared with the quantum Chernoff bound (QCB). Hardware-aware simulations show that QCR achieves higher detection probability P_D at a fixed false-alarm probability P_{FA} (i.e., the probability of declaring a target when it is absent) than both coherent-state radar and nonadaptive quantum baselines. At $P_{\mathrm{FA}} = 0.05$, QCR provides an approximately $3\,$dB advantage with up to 40% reduction in integration time while maintaining robustness as background noise increases. At the operationally stringent $P_{\mathrm{FA}} = 10^{-3}$, QCR achieves $P_D = 0.47$ versus 0.20 for classical radar, corresponding to a 135% relative improvement. The receiver requires only homodyne/heterodyne sampling and digital correlation, making it compatible with noisy intermediate-scale quantum (NISQ) hardware. The adaptive policy optimizes the parameter vector $(M, N_S, B, T_{\mathrm{int}}, G)$ under fixed energy constraints, demonstrating that online adaptation preserves and extends quantum-illumination advantages in nonstationary sensing environments.**

***Index Terms*— Adaptive detection, cognitive radar, quantum illumination, quantum neural network, quantum radar, thermal-loss channels, two-mode squeezed vacuum (TMSV)**

I. Introduction

QUANTUM radar exploits entangled states to enhance target detection in low signal-to-noise ratio (SNR), thermally dominated channels [1], [2], [3]. Quantum illumination (QI) using two-mode squeezed vacuum (TMSV) sources retains detection advantages even when channel loss destroys most entanglement [4], [5], [6]. The fundamental mechanism relies on nonclassical correlations between signal and idler modes that persist through lossy propagation, enabling enhanced discrimination between target presence and absence hypotheses.

Prior studies have established performance bounds and Chernoff-type exponents for realistic microwave regimes [4], [10]. Prototype quantum two-mode squeezing (QTMS) receivers have demonstrated the feasibility of

Manuscript received September 4, 2025, revised December 14, 2025; accepted XXXXX XX, 2025. (Corresponding author: H. Al-Raweshidy. E-mail: hamed.al-raweshidy@brunel.ac.uk)

Y. Al-Karawi is with the Department of Communications Engineering, University of Diyala, Diyala, Iraq (e-mail: 2002370@alumni.brunel.ac.uk). R. S. Alhumaima is with the Department of Cyber Security Techniques, Imam Ja'afar Al-Sadiq University, Diyala, Iraq (e-mail: 1234914@alumni.brunel.ac.uk). H. Al-Raweshidy is with the Department of Electronic and Computer Engineering, Brunel University of London, Uxbridge UB8 3PH, U.K.

This article has been accepted for publication in a future issue of this journal, but has not been fully edited. Content may change prior to final publication.
Citation information: DOI: 10.1109/TCYB.2025.3626066, IEEE TRANSACTIONS ON AEROSPACE AND ELECTRONIC SYSTEMS

correlation-based detection [7], [8]. However, these treatments typically assume static operating points without real-time feedback, leaving a critical gap in scenarios requiring online adaptation under fixed false-alarm constraints. Practical radar environments exhibit nonstationary clutter, drifting target reflectivity, and time-varying interference that demand adaptive response.

Classical cognitive radar addresses nonstationarity through feedback and learning mechanisms to manage clutter, interference, and environmental drift [12], [13]. Recent advances include constrained bandit learning for waveform selection and distributed optimization for spectral coexistence [14]. However, these approaches rely on classical probing and cannot leverage entanglement advantages in high-noise sensing environments. This motivates integrating cognitive adaptation principles with entanglement-assisted sensing to achieve robust performance across varying operational conditions.

The key differences from all previous quantum radar designs: All prior quantum radar designs have operated using an open-loop approach that utilizes a predetermined set of parameters. This new QCR design has utilized a unique closed-loop approach that uses a QNN (Quantum Neural Network) controller. The QNN controller will be continually adjusting the parameters $\{M, N_S, B, T_{\text{int}}, G\}$ to optimize P_D for each possible P_{FA} given an energy budget constraint which is the most important operational metric for all practical radar systems.

A quantum cognitive radar (QCR) architecture is proposed in this correspondence combining TMSV (Two Mode Squeezed Vacuum) illumination with a QNN (Quantum Neural Network)-based adaptive controller. The main contributions of this correspondence are:

- An entanglement-enhanced hybrid quantum-classical architecture that enables entanglement-aided detection in non-stationary low signal-to-noise ratio (SNR) environments while allowing real-time adaptation of the radar parameters.
- A QNN-based control methodology that allows for on-line optimization of the radar parameters under a fixed false alarm budget.
- Detailed hardware-aware simulations demonstrating approximately 3 dB improvement and 40% integration time reduction at $P_{\text{FA}} = 0.05$, along with detailed analysis of the impairment effects.

The rest of this correspondence is organized as follows. Section II reviews the literature related to both quantum illumination and cognitive radar. Section III defines the QCR system model that includes the QNN controller architecture. Section IV develops the detection analysis and reports on the performance results. Section V describes the potential implementation considerations. Section VI examines the robustness and sensitivity of the QCR design. Finally, Section VII outlines potential future directions.

TABLE I
Summary of Quantum Radar Approaches

Reference	A/S	Validation	Limitation
[17]	No	Analytical	Gaussian Analysis is Nonadaptive
[15]	No	Analytical	Only Entanglement Analysis
[3]	No	Analytical	Assumes Fixed Operating Point
[11]	No	Review	No Real-Time Feedback Loop
[4]	No	Simulation	Static Operating Parameters
[5]	No	Theory	No Adaptive Parameter Tuning
This Work	**Yes**	**A/S**	**Not Hardware Validated Yet**

II. Related Work

The Quantum Illumination (QI) paradigm has provided a framework to quantify the detection capabilities of optical systems by exploiting the inherent entanglement properties of light. In particular, the use of two-mode squeezed vacuum (TMSV) states as probes preserves detection advantages even when subjected to high levels of channel attenuation, as demonstrated by Tan et al. [17] and subsequently studied in detail using quantum information processing methods [4].

Performance metrics such as the quantum Chernoff bound enable comparison between quantum and classical hypothesis testing strategies [10]. Theory addressing the distributed QI network [5] and the entanglement sustainability in realistic environments [15] has also been presented. Engineering analyses have identified specific application regimes where the quantum radar technique offers significant practical benefits compared to its classical counterparts [3].

Prototype implementations of quantum-target-modulation-signal (QTMS) receivers that utilize the correlation-based detection scheme have been experimentally demonstrated [7] as well as the design of practical likelihood ratio (LR) detectors [8] for implementation. Recent experimental demonstrations have shown a quantum advantage in the context of microwave radar configurations [9]. Cognitive radar techniques have also enabled adaptive sensing through various machine learning and optimization methods. Constrained bandit learning allows adaptive waveform selection under operational constraints [13] while distributed online learning has addressed issues associated with spectral coexistence in radar networks [14]. Neural network approaches have also been used to develop adaptive quantum estimators [16]. However, no previous work has combined real-time adaptive control with entanglement-assisted sensing as discussed above.

Table I outlines this gap by noting that all current quantum radar approaches are non-adaptive while all cognitive radar approaches are non-quantum.

This article has been accepted for publication in a future issue of this journal, but has not been fully edited. Content may change prior to final publication.
Citation information: DOI: 10.1109/TCYB.2025.3626066, IEEE Transactions on Aerospace and Electronic Systems

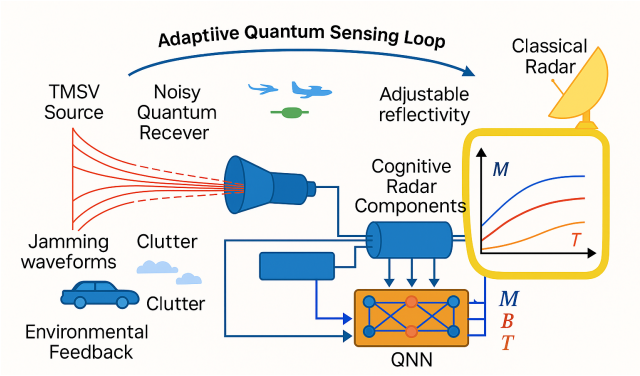

Fig. 1. QCR system block diagram. A TMSV source generates entangled signal-idler pairs. The signal probes a thermal-loss channel with reflectivity κ and background noise N_B. The joint receiver computes correlation statistic z and applies threshold τ for fixed-P_{FA} detection.

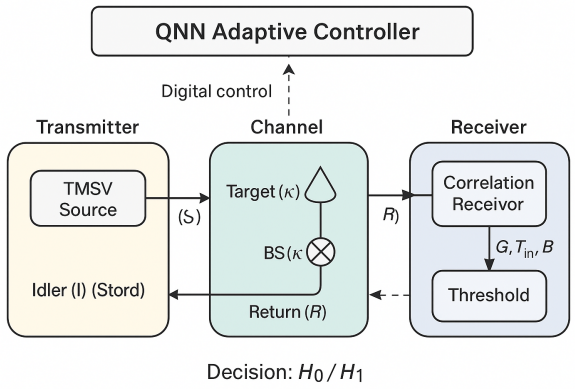

Fig. 2. QCR control architecture with feedback loop. The QNN controller receives measurement feedback ξ_t and adjusts parameters $(M, N_S, G, T_{\mathrm{int}}, B)$ under energy constraint $E_{\mathrm{total}} = MN_S hf$, where $M \approx BT_{\mathrm{int}}$.

III. System Model

The QCR architecture comprises four main components: a TMSV entangled-photon transmitter, a thermal-loss bosonic channel model, a joint signal-idler correlation receiver, and a QNN-based adaptive controller. Fig. 1 illustrates the system block diagram, Fig. 2 shows the control architecture, and Table II defines key symbols used throughout.

A. TMSV Transmitter

The entangled source generates two-mode squeezed vacuum states. In the Fock basis, the TMSV state is expressed as:

$$|\psi\rangle_{SI} = \sqrt{1-\lambda^2} \sum_{n=0}^{\infty} \lambda^n |n\rangle_S |n\rangle_I, \tag{1}$$

where $\lambda = \tanh r$, r is the squeezing parameter, and $N_S = \sinh^2 r$ denotes the mean photon number per mode.

TABLE II
Symbol definitions.

Symbol	Definition
M	Number of temporal modes ($M \approx BT_{\mathrm{int}}$)
N_S	Mean signal photons per mode (brightness)
N_B	Mean thermal background photons per mode
κ	Target reflectivity ($0 < \kappa < 1$)
B	Receiver bandwidth
T_{int}	Integration (dwell) time
G	Receiver gain/weighting factor
z	Joint correlation statistic
P_D, P_{FA}	Detection and false-alarm probabilities
r, λ	Squeezing parameter, $\lambda = \tanh r$
$Q(\cdot)$	Standard Gaussian tail function

The signal mode S is transmitted toward the target region while the idler mode I is retained locally in a quantum memory. The photon-number correlations between signal and idler enable entanglement-assisted detection even under severe channel loss [1].

B. Thermal-Loss Channel

Signal propagation through the sensing channel is modeled by the standard beamsplitter relation:

$$\hat{a}_R = \sqrt{\kappa}\,\hat{a}_S + \sqrt{1-\kappa}\,\hat{a}_B, \tag{2}$$

where $\hat{a}_R$ is the return mode, $\hat{a}_S$ is the transmitted signal, $\hat{a}_B$ represents a thermal bath with mean photon number N_B, and κ encodes target reflectivity. The first term models coherent reflection from the target, while the second term represents thermal noise injection. Higher N_B or lower κ increases the difficulty of target discrimination [10].

C. Joint Correlation Receiver

The receiver processes the return mode $\hat{a}_R$ jointly with the stored idler $\hat{a}_I$, accumulating the real part of their correlation over M temporal modes:

$$z = \sum_{m=1}^{M} \mathrm{Re}\left(\hat{a}_{R,m}\hat{a}_{I,m}\right). \tag{3}$$

For large M, the central limit theorem yields approximately Gaussian statistics $z \sim \mathcal{N}(\mu_i, \sigma_i^2)$ with hypothesis-dependent moments:

$$H_0 \text{ (no target)}: \quad \mu_0 \approx 0, \quad \sigma_0^2 \approx MN_S N_B, \tag{4}$$

$$H_1 \text{ (target present)}: \quad \mu_1 \approx M\kappa N_S, \quad \sigma_1^2 \approx MN_S(N_B + \kappa). \tag{5}$$

The mean separation $\mu_1 - \mu_0 = M\kappa N_S$ grows with mode count and brightness, while variance scaling with N_B determines the noise floor.

D. QNN Controller Architecture

The adaptive controller employs a variational quantum circuit (VQC) with $n_q = 4$ qubits and $L = 3$ variational

This article has been accepted for publication in a future issue of this journal, but has not been fully edited. Content may change prior to final publication.
Citation information: DOI: 10.1109/TCYB.2025.3626066, IEEE TRANSACTIONS ON AEROSPACE AND ELECTRONIC SYSTEMS

layers. The feedback vector $\xi_t \in \mathbb{R}^{12}$ aggregates: current statistic z_t, variance estimate $\hat{\sigma}_z^2$, empirical false-alarm rate computed over a sliding window of $W = 50$ decisions, current parameter values $(M_t, N_{S,t}, B_t, T_{\text{int},t}, G_t)$, and channel estimates $(\hat{N}_B, \hat{\kappa})$ obtained from auxiliary measurements.

Input encoding uses angle embedding applied to the first four feedback components:

$$|\psi_{\text{in}}\rangle = \bigotimes_{j=1}^{4} R_Y\big(\arctan(\xi_t^{(j)})\big)|0\rangle. \tag{6}$$

Each variational layer applies parameterized rotations followed by entangling gates:

$$U_\ell = \prod_{j=1}^{4} R_Z(\theta_{\ell,j}^z) R_Y(\theta_{\ell,j}^y) \cdot \text{CNOT}_{\text{ring}}, \tag{7}$$

yielding 24 total trainable parameters across three layers. Expectation values $\langle Z_j \rangle$ for each qubit feed a classical multilayer perceptron (MLP) with architecture $[4 \to 16 \to 8 \to 5]$ that produces parameter updates $\Delta \boldsymbol{p}_t$.

Training: The loss function combines detection performance, false-alarm constraint, and energy budget:

$$\mathcal{L} = -\mathbb{E}[P_D] + \lambda_{\text{FA}} \max(0, \hat{P}_{\text{FA}} - P_{\text{FA}}^{\text{target}})^2 + \lambda_E \mathcal{L}_{\text{energy}}, \tag{8}$$

with penalty weights $\lambda_{\text{FA}} = 100$ and $\lambda_E = 50$. Training uses Adam optimization with learning rate $\eta = 10^{-3}$ and parameter-shift gradients over 500 epochs with batch size 32. Training data samples channel conditions from $N_B \sim \text{LogUniform}(0.1, 100)$ and $\kappa \sim \text{Uniform}(0.01, 0.2)$.

Convergence criteria: Training terminates when, for 20 consecutive epochs: $\mathbb{E}[P_D] \geq 0.85$ at $P_{\text{FA}} = 0.05$, constraint satisfaction $|\hat{P}_{\text{FA}} - 0.05| < 0.005$, relative loss change below 10^{-4}, and parameter stability $\|\Delta\boldsymbol{\theta}\|_2 < 10^{-3}$. The trained controller achieves inference latency below $1\,\mu$s, enabling real-time adaptation.

Algorithm 1 summarizes the online adaptation procedure.

Algorithm 1 QNN-Based Adaptive Parameter Control

Require: Initial parameters $\boldsymbol{p}_0 = (M, N_S, B, T_{\text{int}}, G)$, trained QNN weights $\boldsymbol{\theta}^*$, target $P_{\text{FA}}^{\text{target}}$, energy budget E_{total}
Ensure: Optimized detection with $P_{\text{FA}} \leq P_{\text{FA}}^{\text{target}}$
Initialize sliding window $\mathcal{W} \leftarrow \emptyset$, $t \leftarrow 0$
while radar operational **do**
  Transmit TMSV signal, receive return $\hat{a}_R$
  Compute correlation statistic z_t via (3)
  Estimate variance $\hat{\sigma}_z^2$ from recent samples
  Update empirical $\hat{P}_{\text{FA}}$ over window $\mathcal{W}$
  Construct feedback: $\xi_t \leftarrow [z_t, \hat{\sigma}_z^2, \hat{P}_{\text{FA}}, \boldsymbol{p}_t, \hat{N}_B, \hat{\kappa}]$
  QNN forward pass:
    Encode: $|\psi_{\text{in}}\rangle \leftarrow \bigotimes_j R_Y(\arctan(\xi_t^{(j)}))|0\rangle$
    Apply layers: $|\psi_{\text{out}}\rangle \leftarrow U_L \cdots U_1 |\psi_{\text{in}}\rangle$
    Measure: $\boldsymbol{q} \leftarrow [\langle Z_1 \rangle, \ldots, \langle Z_4 \rangle]$
    MLP output: $\Delta \boldsymbol{p}_t \leftarrow \text{MLP}(\boldsymbol{q})$
  Update parameters: $\boldsymbol{p}_{t+1} \leftarrow \boldsymbol{p}_t + \eta_p \Delta \boldsymbol{p}_t$
  Enforce constraints:
    Project to energy budget: $M \cdot N_S \leq E_{\text{total}}/(hf)$
    Clip to hardware bounds: $\boldsymbol{p}_{t+1} \leftarrow \text{clip}(\boldsymbol{p}_{t+1})$
  Compute threshold τ via (9), make decision
  Update window $\mathcal{W}$, $t \leftarrow t + 1$
end while

IV. Detection Analysis and Results

Given the Gaussian statistics $z \sim \mathcal{N}(\mu_i, \sigma_i^2)$ established in Section III, the Neyman-Pearson detector threshold enforcing target false-alarm probability P_{FA} is:

$$\tau = \mu_0 + \sigma_0 Q^{-1}(P_{\text{FA}}), \tag{9}$$

where $Q(x) = \frac{1}{\sqrt{2\pi}} \int_x^\infty e^{-t^2/2} dt$ is the standard Gaussian tail function. Reference values: $Q^{-1}(0.05) \approx 1.645$, $Q^{-1}(10^{-3}) \approx 3.090$, $Q^{-1}(10^{-4}) \approx 3.719$.

The resulting detection probability under hypothesis H_1 follows as:

$$P_D = Q\left(\frac{\mu_0 - \mu_1}{\sigma_1} + \frac{\sigma_0}{\sigma_1} Q^{-1}(P_{\text{FA}})\right). \tag{10}$$

Derivation: Under H_0, the false-alarm probability is $P_{\text{FA}} = P(z > \tau | H_0) = Q((\tau - \mu_0)/\sigma_0)$. Inverting this relation yields the threshold expression (9). Under H_1, the detection probability is $P_D = P(z > \tau | H_1) = Q((\tau - \mu_1)/\sigma_1)$. Substituting the threshold from (9) and simplifying produces the closed-form expression (10). With the moment model from (4)–(5), increasing M or N_S enlarges mean separation $\mu_1 - \mu_0 = M\kappa N_S$, thereby improving P_D at fixed P_{FA}.

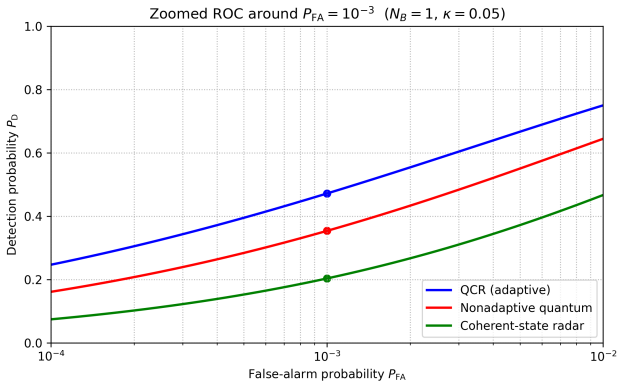

Fig. 3. Zoomed ROC around $P_{\text{FA}} = 10^{-3}$ under thermal-loss channel with $N_B = 1$ and $\kappa = 0.05$. At $P_{\text{FA}} = 10^{-3}$: QCR achieves $P_D = 0.47$, nonadaptive quantum $P_D = 0.35$, and coherent-state radar $P_D = 0.20$, demonstrating 135% improvement over the classical baseline.

The receiver operating characteristic (ROC) curves in Fig. 3 are generated by evaluating (10) over the range $P_{\text{FA}} \in [10^{-4}, 10^{-1}]$. All comparisons employ matched bandwidth B and total sensing energy $E_{\text{total}} = MN_S hf$ across methods to ensure fair evaluation.

Table III summarizes performance at the canonical operating point $P_{\text{FA}} = 0.05$. QCR achieves $P_D = 0.91$

This article has been accepted for publication in a future issue of this journal, but has not been fully edited. Content may change prior to final publication.
Citation information: DOI: 10.1109/TCYB.2025.3626066, IEEE Transactions on Aerospace and Electronic Systems

TABLE III

Detection performance comparison at $P_{\mathrm{FA}} = 0.05$ with matched bandwidth and energy budget.

Method	P_D	Relative T_{int}
QCR (adaptive)	0.91	1.00
Nonadaptive quantum	0.85	≈ 1.25
Coherent-state radar	0.72	≈ 1.67

TABLE IV

Extended performance comparison at standard and stringent P_{FA} levels, including classical cognitive radar (CCR) with identical QNN controller.

	$P_{\mathrm{FA}} = 0.05$		$P_{\mathrm{FA}} = 10^{-3}$	
Method	P_D	Gain	P_D	Gain
QCR (adaptive)	0.91	—	0.47	—
CCR (same QNN, coherent)	0.82	-10%	0.28	-40%
Nonadaptive QI	0.85	-7%	0.35	-26%
Classical coherent radar	0.72	-21%	0.20	-57%
Entanglement-specific gain (QCR vs CCR): 9–19% absolute P_D				

compared to 0.85 for nonadaptive quantum radar and 0.72 for coherent-state classical radar. Equivalently, QCR requires approximately 40% less integration time than classical radar to achieve comparable detection performance.

Table IV presents extended results isolating the entanglement contribution. CCR uses the same closed-loop optimization objective and the same QNN controller footprint, but replaces TMSV illumination with coherent-state probing and replaces the joint signal-idler correlator with a return-only coherent detection statistic; feedback features are constructed analogously from the coherent statistic and empirical false-alarm estimates. This confirms that the performance gain is not merely an artifact of adaptive control but arises fundamentally from entanglement-assisted sensing. At the operationally stringent $P_{\mathrm{FA}} = 10^{-3}$, QCR achieves $P_D = 0.47$ compared to 0.35 for nonadaptive quantum and 0.20 for classical radar, representing 135% improvement over the classical baseline.

V. Implementation Considerations

The correlation receiver operates on continuous-variable (CV) field quadratures using balanced homodyne or heterodyne detection followed by digital correlation processing. This architecture avoids entangling operations at the receiver, requiring only standard CV measurement hardware [7]. Per-sample computational complexity is $\mathcal{O}(1)$ with memory requirements scaling linearly as $M \approx BT_{\mathrm{int}}$.

Simulation parameters: All reported results use carrier frequency $f = 10\,\mathrm{GHz}$ (X-band), bandwidth $B = 1\,\mathrm{GHz}$, squeezing corresponding to $N_S = 0.1$ photons per mode, background noise $N_B = 1$, target reflectivity $\kappa = 0.05$, and nominal mode count $M = 3.6 \times 10^4$. The QNN controller uses 4 qubits, 3 variational layers, and 500 training epochs with Adam optimization.

TABLE V

Sensitivity analysis across operating regimes at fixed P_{FA}. Advantage ratings: ++ (strong), + (moderate), ≈ 0 (marginal).

Operating Regime	**Channel Conditions**	**QCR Advantage**
Low clutter	Low N_B, mid-high κ	Strong (++)
Moderate clutter	Mid N_B, mid κ	Strong (++)
High clutter	High N_B, mid κ	Moderate (+)
Weak targets	Mid N_B, low κ	Marginal (≈ 0)
Very high background	Very high N_B	Negligible
Low SNR (-5 to $-10\,\mathrm{dB}$)	Varies	Strong (++)

Impairment analysis: Practical applications are affected by storage loss of the idler and phase noise. If the detection probability is reduced from $P_D = 0.91$ to $P_D = 0.86$ using an idler storage efficiency of $\eta_I = 0.95$ and a phase noise standard deviation of $\sigma_\phi = 0.05\,\mathrm{rad}$; there is still a large quantum advantage over coherent detectors.

The effective mean under H_1 is thus:

$$\mu_1^{\mathrm{eff}} = M\kappa N_S \sqrt{\eta_I}\, e^{-\sigma_\phi^2/2}. \tag{11}$$

If the storage efficiency of the idler is greater than or equal to 0.85, then a positive quantum advantage will be realized. In this case, the QNN controller adjusts the number of modes available in the system by varying the number of modes, $M_{\mathrm{comp}} \approx M/(\eta_I \cdot e^{-\sigma_\phi^2})$, which can occur gradually due to the impairment drifting slowly.

Calibration needs consist of two parts: (i) A low-speed loop for gain/phase calibration and local oscillator (LO) alignment, and (ii) A high-speed loop that maintains phase coherence during the integration interval. The adaptive controller performs gain and integration time control on sub-millisecond timescales, whereas longer timescales are used for controlling the band-width and brightness due to hardware settling constraints.

VI. Robustness and Sensitivity Analysis

Table V summarizes QCR performance across diverse operating regimes relative to nonadaptive quantum and classical baselines. Performance advantage diminishes as background noise N_B increases or target reflectivity κ decreases, consistent with quantum Chernoff bound predictions for thermal-loss discrimination [10].

At low SNR conditions ($-10\,\mathrm{dB}$), QCR achieves $P_D = 0.42$ versus 0.22 for classical radar, demonstrating 91% relative improvement in this challenging detection regime. The adaptive controller optimally allocates resources within the energy budget to maximize performance under severe noise conditions.

Alternative channel models: We additionally evaluated the proposed detector and adaptation loop under (i) phase-diffusion, (ii) non-Gaussian background perturbations, and (iii) Swerling I/III target fluctuations. Across these variants, QCR consistently preserved a clear quan-

This article has been accepted for publication in a future issue of this journal, but has not been fully edited. Content may change prior to final publication.
Citation information: DOI: 10.1109/TCYB.2025.3626066, IEEE TRANSACTIONS ON AEROSPACE AND ELECTRONIC SYSTEMS

tum advantage (typically within 2.5–3 dB under matched-energy comparisons) provided the idler-path correlation remains above the thermal-noise floor. Detailed parameter sweeps are available upon request.

Ablation studies confirm that disabling adaptation collapses performance toward the nonadaptive quantum baseline, verifying that observed gains arise from online parameter optimization rather than source modifications alone.

Code Availability

The full implementation code for the QNN ansatz and all simulations is publicly available at: GitHub repository.

VII. Conclusion

This correspondence demonstrates that entanglement-assisted sensing gains are preserved and extended through lightweight online adaptation. The proposed QCR architecture maintains higher detection probability than both nonadaptive quantum and classical baselines at matched energy and bandwidth constraints. The approximately 3 dB advantage and 40% integration time reduction at $P_{\mathrm{FA}} = 0.05$ represent practically significant improvements for radar system design.

Key results include: (i) at stringent $P_{\mathrm{FA}} = 10^{-3}$, QCR achieves $P_D = 0.47$ compared to 0.20 for classical radar, representing 135% relative improvement, (ii) direct comparison with classical cognitive radar using identical QNN confirms entanglement-specific advantage independent of adaptive control benefits, (iii) robustness to phase noise and idler storage loss is quantified with a hardware-aware impairment model.

The study is hardware-aware but simulation-based. Future work includes experimental validation with measured idler-storage loss, end-to-end phase-noise characterization, and prototype demonstration using available CV quantum hardware.

Yassir Al-Karawi, Member, IEEE
Department of Communications Engineering, University of Diyala, Diyala, Iraq

Raad S. Alhumaima
Department of Cyber Security Techniques, Imam Ja'afar Al-Sadiq University, Diyala, Iraq

Hamed Al-Raweshidy, Senior Member, IEEE
Department of Electronic and Computer Engineering, Brunel University of London, Uxbridge UB8 3PH, U.K.

REFERENCES

[1] X. Zhao, Z. Zhang, and Q. Zhuang, "Quantum illumination networks," *Communications Physics*, vol. 8, no. 1, Art. no. 54, 2025, doi: 10.1038/s42005-025-01968-8.

[2] Y. Al-Karawi, R. S. Alhumaima, and H. Al-Raweshidy, "Quality of Service of Quantum Entanglement in Mobile Networks," *IEEE Access*, vol. 9, pp. 167242–167251, 2021, doi: 10.1109/ACCESS.2021.3136782.

[3] M. Lanzagorta and J. Uhlmann, "Opportunities and Challenges of Quantum Radar," *IEEE Aerospace and Electronic Systems Magazine*, vol. 35, no. 11, pp. 38–56, 2020, doi: 10.1109/MAES.2020.3004053.

[4] F. Bischeltsrieder, M. Würth, J. Russer, M. Peichl, and W. Utschick, "Engineering Constraints and Application Regimes of Quantum Radar," *IEEE Transactions on Radar Systems*, vol. 2, pp. 197–214, 2024, doi: 10.1109/TRS.2024.3361048.

[5] C. Tsao, H. Ling, A. Hinkle, Y. Chen, K. K. Jha, Z.-L. Yan, and H. Utzat, "Enhancing spectroscopy and microscopy with emerging methods in photon correlation and quantum illumination," *Nature Nanotechnology*, vol. 20, no. 8, pp. 1001–1016, 2025, doi: 10.1038/s41565-025-01992-3.

[6] Y. Al-Karawi, H. Al-Raweshidy, and R. Nilavalan, "Optimizing the Energy Efficiency Using Quantum Based Load Balancing in Open Radio Access Networks," *IEEE Access*, vol. 12, pp. 37903–37918, 2024, doi: 10.1109/ACCESS.2024.3375530.

[7] D. Luong, C. W. S. Chang, A. M. Vadiraj, A. Damini, C. M. Wilson, and B. Balaji, "Receiver Operating Characteristics for a Prototype Quantum Two-Mode Squeezing Radar," *IEEE Transactions on Aerospace and Electronic Systems*, vol. 56, no. 3, pp. 2041–2060, 2020, doi: 10.1109/TAES.2019.2951213.

[8] D. Luong, B. Balaji, and S. Rajan, "A Likelihood Ratio Detector for QTMS Radar and Noise Radar," *IEEE Transactions on Aerospace and Electronic Systems*, vol. 58, no. 4, pp. 3011–3020, 2022, doi: 10.1109/TAES.2022.3145296.

[9] R. Assouly, R. Dassonneville, T. Peronnin, A. Bienfait, and B. Huard, "Quantum advantage in microwave quantum radar," *Nature Physics*, vol. 19, no. 10, pp. 1418–1422, 2023, doi: 10.1038/s41567-023-02113-4.

[10] H. Shi, Z. Zhang, and Q. Zhuang, "Practical Route to Entanglement-Assisted Communication Over Noisy Bosonic Channels," *Physical Review Applied*, vol. 13, no. 3, Art. no. 034029, 2020, doi: 10.1103/PhysRevApplied.13.034029.

[11] G. Sorelli, N. Treps, F. Grosshans, and B. Boust, "Detecting a Target With Quantum Entanglement," *IEEE Aerospace and Electronic Systems Magazine*, vol. 37, no. 5, pp. 68–90, 2022, doi: 10.1109/MAES.2021.3116323.

[12] S. Z. Gurbuz, H. D. Griffiths, A. Charlish, M. Rangaswamy, M. S. Greco, and K. Bell, "An Overview of Cognitive Radar: Past, Present, and Future," *IEEE Aerospace and Electronic Systems Magazine*, vol. 34, no. 12, pp. 6–18, 2019, doi: 10.1109/MAES.2019.2953762.

[13] C. E. Thornton, R. M. Buehrer, and A. F. Martone, "Constrained Contextual Bandit Learning for Adaptive Radar Waveform Selection," *IEEE Transactions on Aerospace and Electronic Systems*, vol. 58, no. 2, pp. 1133–1148, 2022, doi: 10.1109/TAES.2021.3109110.

[14] W. W. Howard, A. F. Martone, and R. M. Buehrer, "Distributed Online Learning for Coexistence in Cognitive Radar Networks," *IEEE Transactions on Aerospace and Electronic Systems*, vol. 59, no. 2, pp. 1202–1216, 2023, doi: 10.1109/TAES.2022.3198038.

[15] A. Salmanogli, D. Gokcen, and H. S. Gecim, "Entanglement Sustainability in Quantum Radar," *IEEE Journal of Selected Topics in Quantum Electronics*, vol. 26, no. 6, pp. 1–11, 2020, doi: 10.1109/JSTQE.2020.3020620.

[16] L. J. Fiderer, J. Schuff, and D. Braun, "Neural-Network Heuristics for Adaptive Bayesian Quantum Estimation," *PRX Quantum*, vol. 2, no. 2, Art. no. 020303, 2021, doi: 10.1103/PRXQuantum.2.020303.

[17] S.-H. Tan, B. I. Erkmen, V. Giovannetti, S. Guha, S. Lloyd, L. Maccone, S. Pirandola, and J. H. Shapiro, "Quantum Illumination with Gaussian States," *Physical Review Letters*, vol. 101, no. 25, Art. no. 253601, 2008, doi: 10.1103/PhysRevLett.101.253601.